Radiative transfer equation inversion: Theory and shape factor models for retrieval of oceanic inherent optical properties

Frank E. Hoge

National Aeronautics and Space Administration, Goddard Space Flight Center, Wallops Flight Facility, Wallops Island, Virginia, USA

Paul E. Lyon

E. G. & G. Inc., Wallops Flight Facility, Wallops Island, Virginia, USA

Curtis D. Mobley and Lydia K. Sundman

Sequoia Scientific, Inc., Redmond, Washington, USA

Received 17 May 2000; revised 5 June 2003; accepted 2 September 2003; published 26 December 2003.

[1] It is shown that the in-water, shape factor formulation of the radiative transfer equation (RTE) (1) yields exact in-air expressions for the remote sensing reflectance R_{rs} and the equivalent remotely sensed reflectance RSR_a and (2) can be configured for inherent optical property (IOP) retrievals using standard linear matrix inversion methods. Inversion of the shape factor RTE is exact in the sense that no approximations are made to the RTE. Thus errors in retrieved IOPs are produced only by uncertainties in (1) the models for the shape factors and related quantities and (2) the IOP models required for inversion. Hydrolight radiative transfer calculations are used to derive analytical models for the necessary backscattering shape factor, radiance shape factor, fractional forward scattering coefficient, ratio of air-to-water mean cosines, and diffuse attenuation coefficient for in-water upwelling radiance. These models predict the various shape factors with accuracies ranging typically from 2 to 20%. Using the modeled shape factors the in-air remotely sensed reflectance RSR_a can be predicted to within 20% of the correct (Hydrolight-computed) values 96% of the time (or ± 0.0005 sr^{-1} 86% of the time) for the synthetic data used to determine the shape factor models. Inversion of this shape factor RTE using field data is a comprehensive study to be published in a later paper. *INDEX TERMS:* 4552 Oceanography: Physical: Ocean optics; 4847 Oceanography: Biological and Chemical: Optics; 4275 Oceanography: General: Remote sensing and electromagnetic processes (0689); 4842 Oceanography: Biological and Chemical: Modeling; *KEYWORDS:* remote sensing, optical oceanography, inverse modeling, radiative transfer theory

Citation: Hoge, F. E., P. E. Lyon, C. D. Mobley, and L. K. Sundman, Radiative transfer equation inversion: Theory and shape factor models for retrieval of oceanic inherent optical properties, *J. Geophys. Res.*, *108*(C12), 3386, doi:10.1029/2000JC000447, 2003.

1. Introduction

[2] Semianalytic radiance models [*Gordon et al.*, 1988; *Morel and Gentili*, 1996] can be readily inverted by linear matrix methods [*Hoge et al.*, 1999a, 1999b, 2001] to provide oceanic inherent optical properties (IOPs). Such inversions are well conditioned [*Hoge and Lyon*, 1996] and promise a powerful method of simultaneously retrieving constituent absorption and backscattering coefficients in the upper surface layer of the world's oceans using satellite data [*Hoge et al.*, 2001; *Hoge and Lyon*, 2002]. However, semianalytic radiance models (1) do not provide an exact framework to account for all possible environmental and viewing conditions [*Weidemann et al.*, 1995] and (2) contain fixed constants that both obscure insight into the physical radiative transfer processes and limit their flexibility.

0148-0227/03/2000JC000447

[3] The radiative transfer equation (RTE) can provide exact inverse solutions, but the RTE is not easily inverted for many remote sensing situations [*Zaneveld*, 1995]. Therefore a specific form of the RTE inversion is investigated, namely a modified version of the shape factor formulation of *Zaneveld* [1995]. Some of the motivation for the work herein comes from the distinct need for highly accurate methods to retrieve the absorption coefficients of the chlorophyll accessory pigment phycoerythrin [*Hoge et al.*, 1999b]. To this end the absorption coefficients of chlorophyll and chromophoric dissolved organic matter (CDOM) must be accurately retrieved; otherwise, weaker absorbing constituents (such as phycoerythrin) will be obscured.

[4] In this paper (1) the shape factor form of the RTE is shown to be readily configured into linear form for simultaneous retrieval of oceanic IOPs using standard matrix methods; (2) the RTE inversion is derived for the principal

"big three" IOPs, namely the phytoplankton absorption coefficient, the CDOM + detritus absorption coefficient, and the total constituent backscattering coefficient; (3) shape factor and related models required for the inversion are developed for backscattering and radiance shape factors, the diffuse attenuation coefficient for upwelling radiance, the ratio of average cosines of the air and water downwelling irradiances, and the fractional forward scattering coefficient; and (4) propagation of errors into the IOP state vector resulting from errors in the data-model matrix and hydrospheric vector as well as shape factor and related models are assessed.

[5] Our ultimate objective is to determine if the shape factor RTE matrix inversion methodology will result in accurate algorithms for application to satellite ocean color data. This paper presents the underlying shape factor RTE theory and develops the needed models for the shape factors and related quantities, while future work will describe comprehensive studies of the shape factor RTE inversion of synthetic and real data.

2. Shape Factor Form of the Radiative Transfer Equation

[6] Establish a Cartesian coordinate system with $+z$ axis vertically downward into the ocean and x and y axes lying within the atmosphere-ocean boundary. In a plane parallel medium without internal sources or inelastic scattering, the radiative transfer equation is

$$\cos\theta \frac{dL(\theta,\phi,z)}{dz} = -c(z)L(\theta,\phi,z) + \int_0^{2\pi}\int_0^{\pi} \beta(\theta,\phi;\theta',\phi';z)L(\theta',\phi',z)\sin\theta'\, d\theta'\, d\phi'. \quad (1)$$

(See notation section for definition of symbols.) *Zaneveld* [1995, 1982] showed that equation (1) can be rewritten in terms of the in-water remotely sensed reflectance (*RSR*) as

$$RSR = \frac{L_u(\theta,\phi,z)}{E_{od}(z)} = \frac{f_b(\theta,\phi,z)\dfrac{b_b(z)}{2\pi}}{-\cos\theta\, k(\theta,\phi,z) + c(z) - f_L(\theta,\phi,z)b_f(z)}, \quad (2)$$

where the dimensionless backscattering shape factor $f_b(\theta, \phi, z)$ is given by

$$f_b(\theta,\phi,z) = \frac{\displaystyle\int_0^{2\pi}\int_0^{\pi/2} \beta(\theta,\phi;\theta',\phi',z)L_d(\theta',\phi',z)\sin\theta' d\theta'\, d\phi'}{\dfrac{b_b}{2\pi}E_{od}(z)}, \quad (3)$$

the dimensionless radiance shape factor $f_L(\theta, \phi, z)$ is given by

$$f_L(\theta,\phi,z) = \frac{\displaystyle\int_0^{2\pi}\int_{\pi/2}^{\pi} \beta(\theta,\phi;\theta',\phi',z)L_u(\theta',\phi',z)\sin\theta'\, d\theta'\, d\phi'}{b_f(z)L_u^{\mathrm{iso}}(z)}, \quad (4)$$

and the diffuse attenuation coefficient for upwelling radiance $k(\theta, \phi, z)$, with units of m^{-1}, is given by

$$k(\theta,\phi,z) = -\frac{1}{L_u(\theta,\phi,z)}\frac{dL_u(\theta,\phi,z)}{dz}. \quad (5)$$

Equation (2) is *Zaneveld*'s [1995] equation (7) and is exact because it is simply a restatement of the RTE (1) for upward directions using definitions (3)–(5). Subscripts d and u appended to the radiance L explicitly remind us that the radiance in equation (3) is downwelling ($0 \le \theta \le \pi/2$), whereas the radiance in equations (4) and (5) is upwelling ($\pi/2 < \theta \le \pi$). (The iso- superscript is discussed below.)

[7] The numerator of the f_b shape factor in equation (3) shows how much downwelling radiance is scattered upward into direction (θ, ϕ). The denominator is the same quantity evaluated for the special case of an isotropic volume scattering function (in which case $\beta = 2b_b/4\pi$). Thus the f_b shape factor is a measure of how much the actual phase function differs from a constant over the backscattering directions. Similarly, the numerator of f_L in equation (4) shows how much the upwelling radiance is forward scattered into direction (θ, ϕ). The denominator is the same quantity evaluated for the special case of an isotropic upwelling radiance distribution whose magnitude is L_u^{iso} and for the special case of an isotropic volume scattering function. Clearly, these shape factors depend both on the IOPs (namely on the volume-scattering function, in this case) and on the ambient radiance distribution, as does the diffuse attenuation coefficient of equation (5). These quantities therefore are unknown terms in equation (2) if equation (2) is to be inverted to obtain the IOPs a and b_b from measured upwelling radiances and downwelling irradiances. The fact that shape factors are unknown prevents the RTE in equation (2) from being inverted unless further assumptions are made about the values of the shape factors. Modeling these unknowns in terms of known quantities is the major focus of this paper.

[8] Equations (1)–(5) are valid at any depth within an arbitrarily stratified water column, but the specific interest herein is remote sensing of near-surface water IOPs. Therefore one needs to relate the quantities in equations (2)–(5), when evaluated just beneath the mean sea surface, to quantities in air just above the sea surface, which can be deduced via in-air remote sensing techniques. Equation (2) can be converted into a form suitable for above-water remote sensing applications as follows. The n-squared law for radiance transmittance across a boundary between two media [*Mobley*, 1994, equation (4.21)] can be used to convert the in-water upwelling radiance just beneath the sea surface, $L_u(\theta, \phi, z = 0)$, to the water-leaving radiance in-air just above the sea surface, $L_{ua}(\theta_a, \phi)$:

$$L_u(\theta,\phi,z=0) = \frac{n_w^2}{t}L_{ua}(\theta_a,\phi). \quad (6)$$

Subscript a denotes values in air, just above the mean sea surface; depth $z = 0$ denotes values in water, just beneath the sea surface. The in-air polar angle θ_a associated with $L_{ua}(\theta_a, \phi)$ is the refracted viewing angle above the sea surface obtained by applying Snell's law to the in-water

angle θ. The downwelling scalar irradiance $E_{\mathrm{od}}(z)$ is converted to the downwelling plane irradiance $E_{\mathrm{d}}(z)$ via the mean cosine of the downwelling radiance, $\bar{\mu}_{\mathrm{d}}$: $E_{\mathrm{od}}(z) = E_{\mathrm{d}}(z)/\bar{\mu}_d$. The plane irradiance just beneath the sea surface can be related to the in-air value via [*Mobley*, 1994, equation (7.19)] $E_{\mathrm{d}}(z = 0) = E_{\mathrm{da}}\bar{t}/(1 + rR)$. Combining these results gives [*Mobley*, 1994, equation (10.27)]

$$\frac{L_u(\theta,\phi,z=0)}{E_{od}(z=0)} = \frac{n_w^2(1-rR)\bar{\mu}_d}{t\,\bar{t}}\,\frac{L_{ua}(\theta_a,\phi)}{E_{da}}. \tag{7}$$

In equation (7), define $M \equiv [(t\,\bar{t})/[(1 - rR)n_{\mathrm{w}}^2]$. For a wide range of sky and sea surface conditions and for viewing directions relevant to remote sensing, M lies in the range of 0.53 to 0.55 [*Mobley*, 1994; *Hoge and Lyon*, 1996; *Hoge et al.*, 1999a, 1999b; *Morel and Gentili*, 1996]. Thus M can be approximated as $M \approx 0.54$, with an error of less than 2%. Using equation (7) and partitioning the beam attenuation coefficient as $c(z) = a(z) + b_f(z) + b_b(z)$, equation (2) becomes

$$R_{rs} = \frac{L_{ua}(\theta_a,\phi)}{E_{da}} = \frac{M f_b(\theta,\phi,0)\, b_b(0)/[2\pi\,\bar{\mu}_d(0)]}{-k(\theta,\phi,0)\cos\theta + b_f(0)[1 - f_L(\theta,\phi,0)] + a(0) + b_b(0)}. \tag{8}$$

Except for the small error associated with the assumed value for M, equation (8) remains an exact RTE expression for the in-air remote sensing reflectance, R_{rs}, just above the sea surface. The remote sensing reflectance is the quantity used as the basis for ocean color remote sensing by the Sea-viewing Wide Field-of-view Sensor (SeaWiFS) [*O'Reilly et al.*, 1998; *Hoge et al.*, 2001; *Hoge and Lyon*, 2002] and airborne systems [*Davis et al.*, 2002; *Hoge et al.*, 1999a, 1999b] systems. R_{rs} can be obtained from at-sensor radiances after atmospheric correction; for our purposes here it is therefore considered known. As noted by *Zaneveld* [1995], it is desirable to use RSR_a, the in-air value of RSR, rather than R_{rs} because the scalar irradiance E_{od} is less sensitive to solar zenith angle effects than is the plane irradiance E_{d}. Thus use $RSR_a = \bar{\mu}_{da}R_{rs}$ to rewrite equation (8) as

$$RSR_a = \frac{L_{ua}(\theta_a,\phi)}{E_{oda}} = \frac{M\,\frac{f_b(\theta,\phi,0)}{2\pi}\,\frac{\bar{\mu}_{da}}{\bar{\mu}_d(0)}\,b_b(0)}{-k(\theta,\phi,0)\cos\theta + b_f(0)[1 - f_L(\theta,\phi,0)] + a(0) + b_b(0)}. \tag{9}$$

The simplicity of *Zaneveld*'s [1995] original in-water RSR formulation remains in this equation for RSR_a, except for M and the $\bar{\mu}_{da}/\bar{\mu}_d$ ratio for the downwelling light field. As a practical matter, equation (8) is presently more easily applied to oceanic field data because the in-air downwelling plane irradiance is more generally available, but there are no instrumental barriers to using scalar irradiance as in equation (9).

[9] To further simplify equation (9) for later use, define the first term in the denominator as

$$D_L(\theta,\phi,0) = -k(\theta,\phi,0)\cos\theta. \tag{10}$$

Call D_{L} the radiance derivative term because it is a measure of the depth rate of change of the upwelling radiance, as seen in equation (5). Define the second term in the denominator as

$$B_f(\theta,\phi,0) \equiv b_f(0)[1 - f_L(\theta,\phi,0)]. \tag{11}$$

The shape factor f_L varies from 0.963 to 1.152 for nadir viewing [*Weidemann et al.*, 1995; *Zaneveld*, 1995]; thus B_f ranges from $0.037b_f$ to $-0.152b_f$, which is a small fraction of the forward scattering coefficient b_f. Therefore call B_f the fractional forward scattering coefficient. Thus b_f and f_L are found in a combination in which one (f_L) serves to reduce the size of the other (b_f). Finally, define the mean cosine ratio as

$$R_{\mu} = \frac{\bar{\mu}_{da}}{\bar{\mu}_d\,(0)}. \tag{12}$$

Using definitions (10)–(12), equation (9) becomes

$$RSR_a(\theta_a,\phi) = \frac{L_{ua}(\theta_a,\phi)}{E_{oda}} = \frac{M\,\frac{f_b(\theta,\phi,0)}{2\pi}R_{\mu}\,b_b(0)}{D_L(\theta,\phi,0) + B_f(\theta,\phi,0) + a(0) + b_b(0)}. \tag{13}$$

Equations (8), (9), and (13) are each called the shape factor form of the RTE. Equation (13) is addressed hereafter. The ultimate goal is to use equation (13) to relate the unknown absorption and backscattering coefficients just beneath the sea surface to the known remotely sensed reflectance and other known quantities. As noted above, M = 0.54. However, the four quantities f_b, R_{μ}, D_L, and B_f (or, equivalently, f_b, R_{μ}, k, and b_f (1 − f_L) as seen in equation (9) and for brevity call all of these quantities shape factors) are unknown. The shape factors depend in complicated ways on the water column IOPs, environmental conditions (sky radiance and sea state), and viewing geometry (Sun zenith angle and viewing direction). In section 4 the shape factors are modeled, so that they too can be considered known in equation (13).

3. Linear Form of the Radiative Transfer Equation and Its Inversion

[10] The in-air RSR_a of equation (13) immediately yields the fundamental linear form of the RTE,

$$a(0) + b_b(0)V + D_L + B_f = 0, \tag{14}$$

where

$$V(\theta,\phi,0) = 1 - \frac{M\,\frac{f_b(\theta,\phi,0)}{2\pi}R_{\mu}}{\frac{L_{ua}(\theta_a,\phi)}{E_{oda}}}. \tag{15}$$

V is called the backscattering enhancement factor.

[11] Next, partition the total absorption coefficient into contributions by pure water, phytoplankton, and CDOM

plus detritus. Similarly, the backscattering coefficient is written as the sum of contributions by pure seawater and by particulate matter. It is easy to show [*Hoge and Lyon*, 1996; *Hoge et al.*, 1999a, 1999b] that the equation describing the desired phytoplankton absorption coefficient a_{ph}, CDOM + detritus absorption coefficient a_d, and total constituent backscattering coefficient b_{bt} resulting from equation (14) is

$$a_{ph}(\lambda_i) + a_d(\lambda_i) + b_{bt}(\lambda_i)V = -a_w(\lambda_i) - b_{bw}(\lambda_i)V - D_L - B_f. \tag{16}$$

The wavelength dependency of the IOPs is now shown explicitly, while the depth and angular dependencies have been suppressed for clarity. Note that the observed water-leaving radiances L_{ua} occur on both sides of the equation (within V). The pure water absorption a_w is known from *Pope and Fry* [1997], and the water backscattering coefficient b_{bw} is given by *Smith and Baker* [1981]. The right-hand side of equation (16) is therefore known, given the shape factors and a measurement of $RSR_a(\lambda_i)$. This linear form of the RTE is still exact in the sense that no approximations have been made to the RTE, but clearly, the IOP retrieval accuracy will be determined by the accuracy of the shape factor models.

[12] Given the water-leaving radiance at three wavelengths, equation (16) still cannot be solved for the "big three" IOPs, $a_{ph}(\lambda_i)$, $a_d(\lambda_i)$, and $b_{bt}(\lambda_i)$, because each measurement of $RSR_a(\lambda_i)$ yields an equation with three unknown IOPs. However, it is easy to show that a consistent solution is available by introducing spectral models for $a_{ph}(\lambda_i)$, $a_d(\lambda_i)$, and $b_{bt}(\lambda_i)$ [*Hoge and Lyon*, 1996; *Hoge et al.*, 1999a, 1999b]. Substitution of such spectral models for $a_{ph}(\lambda_i)$, $a_d(\lambda_i)$, and $b_{bt}(\lambda_i)$ into equation (16) yields

$$\begin{aligned} a_{ph}(\lambda_g)\exp\left[-\frac{(\lambda_i-\lambda_g)^2}{2g^2}\right] \\ + a_d(\lambda_d)\exp[-S(\lambda_i-\lambda_d)] + b_{bt}(\lambda_b)\left(\frac{\lambda_b}{\lambda_i}\right)^n V \\ = -a_w(\lambda_i) - b_{bw}(\lambda_i)V - D_L - B_f. \end{aligned} \tag{17}$$

Equation (17) now has only three unknowns, $a_{ph}(\lambda_g)$, $a_d(\lambda_d)$, and $b_{bt}(\lambda_b)$, so that the system is solvable given measurements of $RSR_a(\lambda_i)$ at three wavelengths. This linear form of the radiative transfer equation remains exact and precise, but the uncertainty in the retrieved IOPs is now additionally influenced by the uncertainty in the IOP models [*Hoge et al.*, 1999a, 1999b] (in addition to the shape factors).

[13] At their respective reference wavelengths, λ_g, λ_d, and λ_b, the IOPs $a_{ph}(\lambda_g)$, $a_d(\lambda_d)$, and $b_{bt}(\lambda_b)$, are linearly related to the column matrix, or vector, containing the hydrospheric constants (sea water absorption and backscattering), radiances, and the shape factors. (It is easy to see from equation (16) that it is, in principle, possible to concurrently solve for the radiance derivative term $D_L(\lambda_i)$ and/or for the fractional forward scattering coefficient, B_f, in addition to the IOPs, given measurements of $RSR_a(\lambda_i)$ at additional wavelengths. However, the IOP models then must be of sufficient accuracy at yet a fourth and/or fifth wavelength, and the required wavelength dependency of these models was not a focus of this study. Therefore such retrievals are beyond the scope of this initial RTE inversion work.) Equation (17) is very similar to the one used to analyze the effect of radiance errors and model uncertainties upon IOPs [*Hoge and Lyon*, 1996], and to retrieve IOPs from atmospherically corrected airborne and satellite upwelling radiances [*Hoge et al.*, 1999a, 1999b, 2001] when retrieved by semianalytic radiance model inversion. Equation (17) can therefore be written in matrix form as

$$\boldsymbol{D}\boldsymbol{p} = \boldsymbol{h}. \tag{18}$$

Here the hydrospheric vector $\boldsymbol{h}$ is given by the right-hand side of equation (17). The IOP state vector is $\boldsymbol{p} = [a_{ph}(\lambda_g), a_d(\lambda_d), b_{bt}(\lambda_b)]^T$, where T denotes the transpose and $\boldsymbol{D}$ is the data-model matrix [*Hoge and Lyon*, 1996; *Hoge et al.*, 1999a, 1999b, 2001], which also contains shape factors. The IOPs are immediately determined from $\boldsymbol{p} = \boldsymbol{D}^{-1}\boldsymbol{h}$.

[14] The uncertainties in the IOP state vector $\boldsymbol{p}$ can be analyzed in a manner similar to other linear inversions [*Hoge and Lyon*, 1996]. Since $\boldsymbol{p} = \boldsymbol{D}^{-1}\boldsymbol{h}$, both $\boldsymbol{D}$ and $\boldsymbol{h}$ determine $\boldsymbol{p}$ and the errors that propagate into $\boldsymbol{p}$. Because the backscattering shape factor f_b is always found within $\boldsymbol{D}$, f_b influences the propagation of errors into the IOPs more so than the remaining factors. The discussion of the uncertainties in the IOP state vector $\boldsymbol{p}$ caused by possible singularity of $\boldsymbol{D}^{-1}$ and by perturbations in $\boldsymbol{D}$ somewhat parallels a similar previous discussion [*Hoge and Lyon*, 1996] and is briefly addressed in a later section herein.

4. Models for Shape Factors and Related Quantities

[15] Inversion of equation (17) using remotely sensed ocean color data requires knowledge of V, D_L, and B_f. These quantities in turn depend on the shape factors f_b and f_L, the diffuse attenuation coefficient k, and the mean cosine ratio R_μ, as defined above. For ease of comparison with previous work on shape factors [*Weidemann et al.*, 1995] and to reveal the underlying physics as much as possible, explicit models for f_b, f_L, k, and R_μ, are given rather than D_L and B_f. For notational convenience, let X_i with i = 1, 2, 3, and 4 denote f_b, f_L, k, and R_μ, respectively.

[16] Because shape factors, diffuse attenuation functions, and mean cosines all depend on the ambient radiance, they depend implicitly on the solar zenith angle and viewing direction, as well as on the IOPs. The solar angle and viewing direction are known in any particular remote sensing situation; these geometric quantities are thus available for modeling the X_i in terms of known quantities. However, the IOPs are unknown. Explicit inversions of the RTE (to obtain the IOPs) excludes the IOPs from the models for the X_i. However, an implicit, or iterative, inversion of the RTE, can include the retrieved IOPs in the X_i models, for the following reason. In an iterative inversion, one starts with an initial guess for the X_i, derived either from models that do not include IOPs or from physical intuition. (For example, a reasonable initial guess for f_b would be 1, the value corresponding to a constant phase function. Similarly, f_L = 1, k = 0, and R_μ = 1 would be acceptable initial guesses.) Using the initial guesses for the X_i, the RTE is

Table 1. Parameters and Their Values Used to Generate the Original Database of 184,800 Records[a]

Parameter	Values Used in Hydrolight Runs
chlorophyll concentration, *Chl*	**0.1**, **0.5**, **1.0**, **5.0**, **10.0** mg m^{-3}
solar zenith angle, θ_s	**0.0**, **10**, **20**, **30**, **40**, **60** degrees
wind speed	**0**, 10 m s^{-1}
cloud cover	**0**, 100%, i.e., clear sky and solid overcast
wavelength, λ	**412**, **426**, **440**, **465**, **490**, **522.5**, **555**, **612**, **670**, **685** nm
polar viewing angle θ_v (in water, relative to the zenith)	**0.0**, **10**, **20**, **30**, **40**, 50, 60 degrees
azimuthal viewing angle ϕ_v (relative to Sun)	0, **90**, 180 degrees
depth, z	**0**, 0.5, 1, 1.5, 2, 2.5, 3, 3.5, 4, 4.5, 5 m

[a]The values shown in bold correspond to the 1,500 records in the remote sensing database.

inverted to obtain initial values for $a_{ph}(\lambda_g)$, $a_d(\lambda_d)$, and $b_{bt}(\lambda_b)$, from which the IOPs $a = a_t + a_w = a_{ph} + a_d + a_w$ and $b_b = b_{bt} + b_{bw}$ can be obtained at all wavelengths via the IOP models seen in equation (17). The X_i models developed below are based on an assumed phase function for particle scattering. Taking the particle phase function as known, the total constituent (particle) backscattering fraction $B_t = b_{bt}/b_t$ is also known. Thus the total constituent forward scattering coefficient b_{ft} can be obtained from the recovered b_{bt} and B_t: $b_{ft} = b_{bt}(1 - B_t)$. The total beam attenuation coefficient is then known from $c = a + b_{ft} + b_{bt} + b_w$. Therefore models are developed for the X_i that depend both on the known geometrical (viewing direction (subscript v), solar direction (subscript s), and physical (wind speed, wavelength)) parameters, as well as on certain IOPs (namely, a, c, and b_b).

4.1. Database

[17] To begin the analysis, 120 Hydrolight [*Mobley*, 2001a, 2001b] runs were made using its IOP model for case 1 waters and the Petzold ''average particle'' phase function [*Mobley et al.*, 1993] for scattering by the particles. This case 1 IOP model is a two-component model: pure water plus ''everything else.'' The non-water absorption and scattering coefficients are parameterized in terms of the chlorophyll concentration according to commonly used models by *Mobley* [1994, equations (3.27) and (3.40)]. The input for these runs covered a wide range of chlorophyll concentrations, solar zenith angles, cloud covers, and wind speeds. Each Hydrolight run generated output at various wavelengths, depths, and viewing directions. The resulting database potentially contains millions of records, where one record corresponds to a particular set of input values, output values for a particular viewing geometry, wavelength, depth, etc., and the values of the four X_i. Some of these records are not of great interest, for example, records whose azimuthal viewing directions ϕ_v differ by only 15 degrees (the resolution of ϕ_v in the standard version of Hydrolight). Therefore selected records were used to generate a database of more manageable size but one that still covers the range of parameter values relevant to most remote sensing. Table 1 shows the input and output values in this database, which was used in the initial investigation of the functional forms of the X_i. Each of the four X_i was computed for each parameter combination represented in Table 1.

[18] First, the sensitivity of the X_i to the various parameters (wind speed, viewing direction, IOPs, etc.) available for construction of models for the X_i was examined. It was found that the surface wind speed has a negligible effect on each of the X_i (less than 1% difference in X_i for the 0 and 10 m s^{-1} wind speeds, with all else being equal). Thus the wind speed was not considered in subsequent modeling. Likewise, for similar reasons, only the clear-sky data, which are of greatest interest for remote sensing applications were included. As noted above, for remote sensing applications the shape factors X_i need evaluation only at depth $z = 0$. (Note, however, that the values of the X_i at $z = 0$ incorporate the effects of all the absorption and multiple scattering occurring throughout the entire water column.) Thus only output from the Hydrolight runs at $z = 0$ was retained. The original database included records generated for azimuthal viewing angles of $\phi_v = 0$ (looking toward the Sun) and $\phi_v = 180$ degrees (looking away from the Sun). Most remote sensing is, or can be, accommodated at azimuthal angles of $\phi_v \approx 90$ degrees, which minimizes Sun glint and instrument self shading. Thus only the records corresponding to $\phi_v = 90$ degrees were included. Likewise, remote sensing generally uses in-air nadir viewing directions θ_{va} of less than 60 degrees, which correspond to in-water angles $\theta_v \leq 40$ degrees. Eliminating the larger in-water nadir viewing angles ($\theta_v = 50$ and 60 degrees in Table 1) gives a final ''remote sensing'' data set of 1500 records, which was used to determine models for the X_i. The parameter values corresponding to this remote sensing database are shown in bold in Table 1.

4.2. Determining Functional Forms

[19] Let P_k with $k = 1,\ldots,N_k$, denote the parameters (wavelength, viewing direction, IOPs, etc.) to be used in modeling the X_i. These parameters include those seen in Table 1, as well as the absorption, scattering, and backscattering coefficients (which are functions of the chlorophyll concentration if case 1 water is assumed).

[20] The simplest possible model for the X_i is a linear function of the P_k:

$$X_i = \sum_{k=1}^{N_k} \alpha_{ik} P_k, \quad i = 1, \ldots, 4 \; . \tag{19}$$

The α_{ik} are fitting coefficients whose values are to be determined; a different set of coefficients is needed for each factor X_i. That is, a large linear least squares problem was initiated to determine if this model was adequate to fit the various factors. Not surprisingly, the fits were unsatisfactory. In other words, the ocean is more complicated than equation (19).

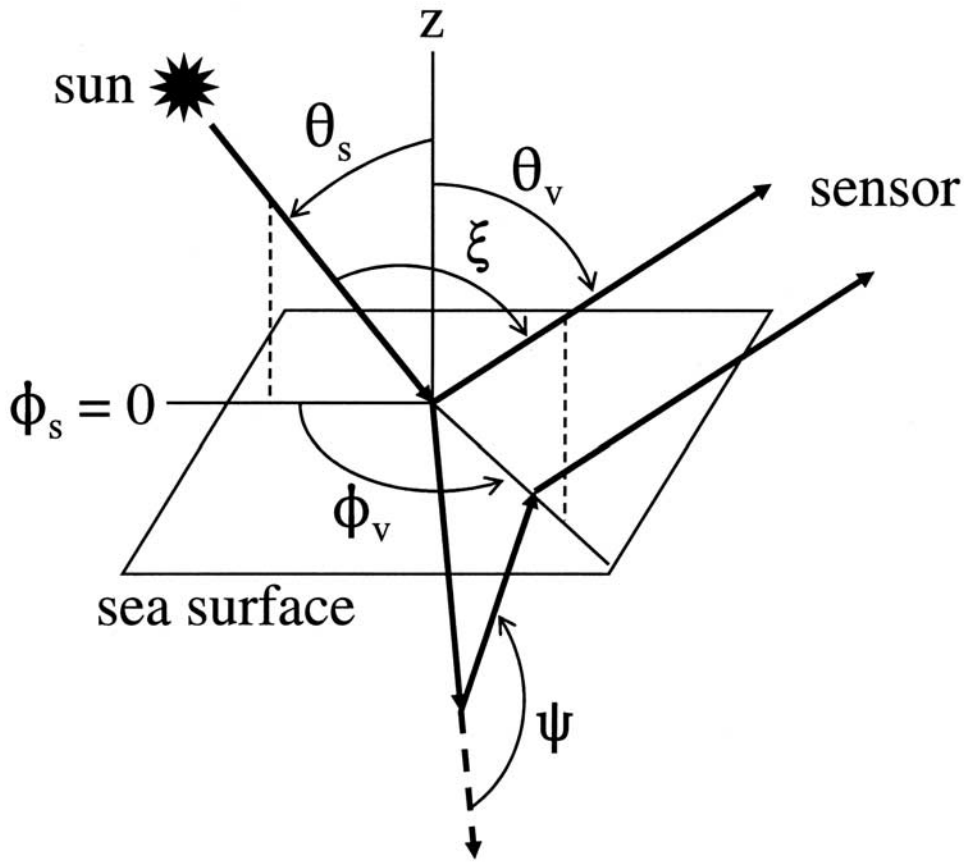

Figure 1. Sun, sensor, and single-scattering geometry. Equation (1) measures the polar angle θ from the nadir with +z downward, and Hydrolight computes in this coordinate system as well, but the above-surface solar and viewing directions are shown for convenience as being measured from the zenith.

[21] The goal then became to develop models that are nonlinear in the parameters but still reflect the underlying physics of the X_i. Thus replace equation (19) by

$$X_i = \sum_{k=1}^{N(i)} F_{ik}(\{P_k\}, \{\alpha_{ik}\}). \tag{20}$$

This notation means that each function F_{ik} will contain some subset of the parameters P_k and will have its own set of fitting coefficients. For example, as shall be seen in the next section, the model for f_b will contain terms involving the scattering-to-backscattering ratio and a nonlinear function of the three geometric parameters (θ_s, θ_v, and ϕ_v), with four fitting coefficients in all.

4.3. Model for f_b

[22] To obtain initial guidance about the possible functional form for an f_b model, single-scattering theory was first used to evaluate the definition of f_b seen in equation (3). According to the single-scattering approximation (SSA), the downwelling radiance is [*Gordon*, 1994, equation (1.30)]

$$L_d(\theta', \phi', z) = E_{od}\delta(\mu' - \mu_s)\delta(\phi' - \phi_s)e^{-cz/\mu_s}, \tag{21}$$

where $\mu = \cos\theta$ and (μ_s, ϕ_s) denote the in-water direction of the Sun's direct beam as refracted through a level sea surface; δ is the Dirac delta function. Inserting equation (21) into equation (3), integrating, and evaluating the result at $z = 0$ gives

$$f_b \approx 2\pi \frac{b}{b_b}\widetilde{\beta}(\mu_s, \phi_s, \mu, \phi). \tag{22}$$

Note that for isotropic scattering, $\widetilde{\beta} = 1/4\pi$, $b = 2b_b$, giving $f_b = 1$, as expected. As the phase function becomes more anisotropic, b/b_b increases, and f_b increases. In equation (22) the phase function indicates that to first order, f_b involves downwelling radiance that is singly scattered from the Sun's direct beam into the viewing direction. In remote sensing applications the total phase function (water plus particles) will be unknown, but for any given phase function the contribution to f_b will depend on the scattering angle ψ corresponding to the Sun's downward beam being scattered into the upward viewing direction. This scattering angle is equivalent to the easily computed Sun sensor-included angle ξ, as shown in Figure 1. Given the Sun's location (θ_s; $\phi_s = 0$), the viewing direction (θ_v, ϕ_v), ξ is given by

$$\cos\xi = \cos\theta_s \cos\theta_v + \sin\theta_s \sin\theta_v \cos\phi_v.$$

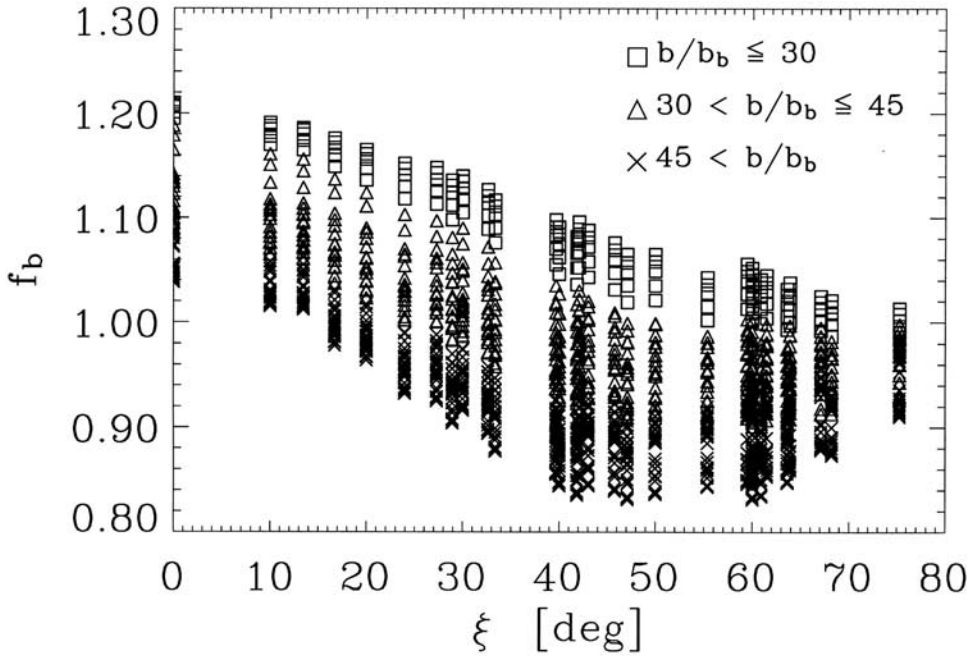

Figure 2. Values of f_b plotted as a function of Sun sensor included angle ξ and coded to show the dependence on b/b_b.

Thus, as a preliminary functional form for the f_b model, consider the estimated backscattering shape factor

$$\hat{f}_b \propto \frac{b}{b_b}\Xi(\xi),$$

where $\Xi(\xi)$ is a function of angle ξ whose form is to be determined.

[23] Figure 2 shows the 1,500 values of f_b in the remote sensing database plotted as a function of ξ and b/b_b. This figure suggests that a cosine function may capture the ξ dependence. Thus construct a model of the form

$$\hat{f}_b = \alpha_1 + \alpha_2 \frac{b}{b_b}\cos(\alpha_3 \xi), \tag{23}$$

where α_1, α_2, and α_3 are fitting coefficients (the α_{ik} of equation (20) for model $i = 1$) whose values are to be determined by minimizing the squared difference between $\hat{f}_b$ and f_b for the 1,500 values in the remote sensing database. Note from the points in Figure 2 that f_b is largest for small b/b_b, and vice versa, which is contrary to the behavior predicted by equation (22). This reversal may be due to the dominance of multiple scattering in ocean waters, but further investigations would be necessary to understand this discrepancy between the SSA predictions and the Hydrolight predictions, which include all orders of multiple scattering and other effects not included in the SSA. In any case, there is a clear dependence on b/b_b, which can be modeled.

[24] The best fit coefficients α_j in equation (23) were determined by least-squares minimization using a variety of numerical techniques appropriate for nonlinear functions. After comparing the model predictions $\hat{f}_b$ with the actual f_b values, it was seen that not all of the b/b_b dependence was captured by the model of equation (23). Some experimentation showed that the remaining b/b_b dependence could be accounted for by adding another term proportional to b/b_b. Thus the final f_b took the form

$$\begin{aligned}\hat{f}_b &= \alpha_1 + \alpha_2 \frac{b}{b_b}\cos(\alpha_3 \xi) + \alpha_4 \frac{b}{b_b} \\ &= \alpha_1 + \alpha_4 \frac{b}{b_b}\left[1 + \frac{\alpha_2}{\alpha_4}\cos(\alpha_3 \xi)\right].\end{aligned} \tag{24}$$

Equation (24) shows that the additive term is equivalent to keeping the general form of the model suggested by the SSA, but picking a different angular function $\Xi(\xi)$. The complicated dependence of f_b on b/b_b and ξ is not surprising if one remembers that the $\Xi(\xi)$ function is fundamentally an attempt to parameterize the unknown phase function effects for a given Sun and viewing geometry; thus the scattering and geometric effects are not independent. The final set of fitting coefficients for the model in equation (24) is shown in Table 2.

[25] Figure 3 shows the model and actual f_b values. The dashed lines are the 5% error bounds. Using the model of equation (24), 96.3% of the predicted values are within 5% of the correct value; the linear correlation coefficient between the model and actual points is $r = 0.955$. There is no systematic dependence on b/b_b or ξ of the model

Table 2. Best Fit Coefficients for the f_b Model of Equation (24)

Coefficient	Value
α_1	1.2077
α_2	0.001977
α_3	3.3790
α_4	−0.004863

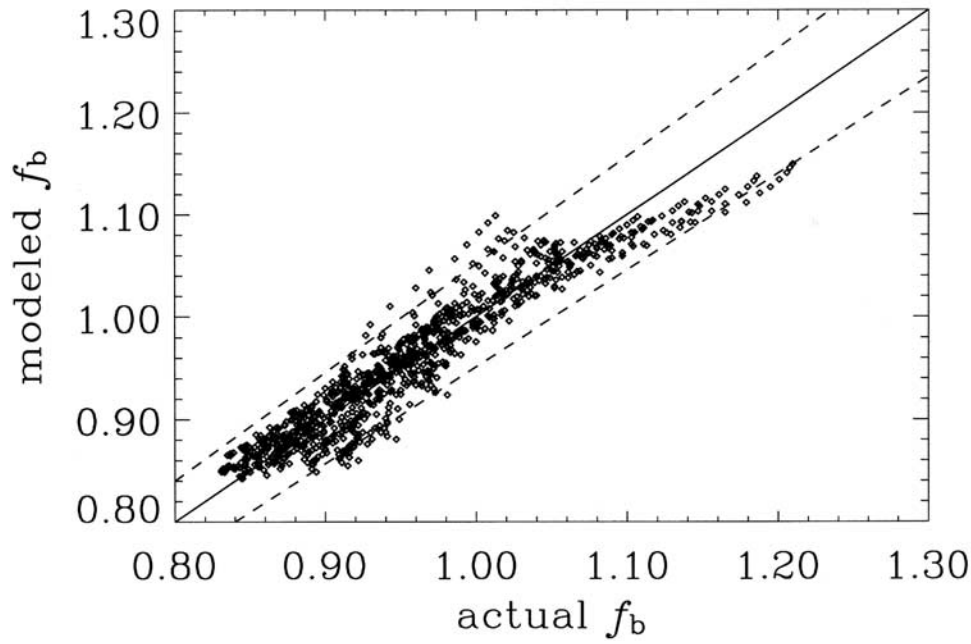

Figure 3. Comparison of modeled and actual f_b values, using the model of equation (24). Here 96.3% of the modeled values lie within the dashed lines, which represent values with 5% of the correct value; the model-actual correlation coefficient is $r = 0.955$.

discrepancies seen in the individual points of Figure 3. It would be possible to continue adding ad hoc terms in other variables to equation (24) and perhaps reduce the model-data discrepancy even more. However, such a process is likely to deviate from physical foundations, with the end result that the final model would not be applicable beyond the exact conditions used to generate the present remote sensing data set. For this initial study it is best to be content with the simple model of equation (24).

4.4. Model for $B_f = b_f[1 - f_L]$

[26] Since b_f is an IOP the model required for B_f is f_L. Just as with f_b, use the SSA for guidance as to the general form of the model for f_L. In the SSA the upwelling radiance is [*Gordon*, 1994, equation (1.32)]

$$L_u(\mu', \phi', z) = \frac{b}{c} E_d(0) \tilde{\beta}(\mu_s, \phi_s, \mu', \phi') \frac{1}{\mu_s - \mu'} e^{-cz/\mu_s}. \qquad (25)$$

Note that $\mu_s > 0$ and $\mu' < 0$. Inserting this SSA radiance into equation (4), the definition of f_L, integrating, and setting $z = 0$ gives

$$f_L \approx \frac{b_2 E_d(0)}{b_f c L_u^{iso}} \int_0^{2\pi} \int_0^{-1} \tilde{\beta}(\mu', \phi', \mu, \phi) \tilde{\beta}(\mu_s, \phi_s, \mu', \phi') \frac{1}{\mu_s - \mu'} d\mu' \, d\phi'.$$

In most ocean waters, $b \approx b_f$. However, further simplification is difficult. The remaining integrals describe how the Sun's downwelling direct beam is first scattered upward and then scattered again into the viewing direction. The most that can be said is that this is some function of the scattering phase function and the viewing geometry. As with f_b, this function was parameterized in terms of the Sun sensor included angle ξ via a model of the form

$$\hat{f}_L \propto \frac{b}{c} \Xi(\xi).$$

Unfortunately, plots of f_L similar to Figure 2 did not suggest a clear functional form for $\Xi(\xi)$ or show any significant dependence on b/c. This failure of the SSA to provide a functional form for f_L is not surprising because f_L inherently involves at least two scatterings, and multiple scattering can be expected to make an important contribution to the upwelling radiance.

[27] Linear correlations between f_L and the various available fitting parameters were then examined. The results are seen in Table 3.

[28] The only potential model parameter that correlates well with f_L is the solar zenith angle θ_s. A plot of f_L versus θ_s

Table 3. Correlation Between the Radiance Shape Factor f_L and Various Parameters

Parameter	Correlation Coef. r With f_L
Absorption coefficient a	0.291
Scattering coefficient b	0.205
Albedo of single scattering b/c	−0.076
Backscattering coef b_b	0.180
Forward scattering coef b_f	0.206
Backscattering fraction b_b/b	−0.343
Forward scattering fraction b_f/b	0.343
Backscattering to absorption b_b/a	−0.231
Wavelength λ	0.210
Solar zenith angle θ_s	0.778
Polar viewing angle θ_v	−0.006
Sun sensor included angle ξ	−0.562

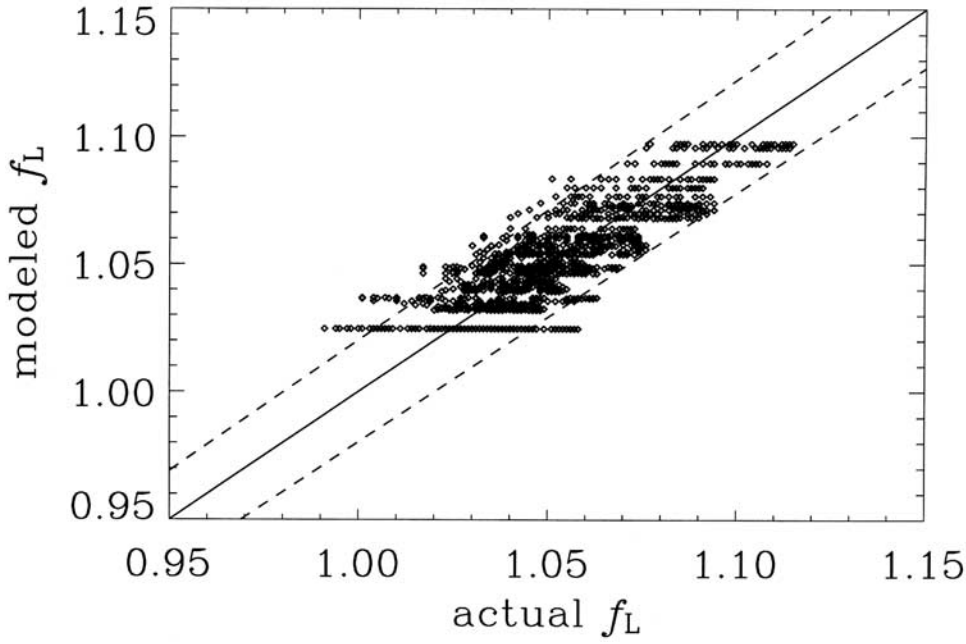

Figure 4. Comparison of modeled and actual f_L values, using the model of equation (24). Here 93.0% of the modeled values lie within the dashed lines, which represent values with 2% of the correct value; the model-actual correlation coefficient is $r = 0.829$.

suggested a sine function for θ_s (although a simple linear function is almost as good). Thus a model of the form $\hat{f}_L = \alpha_5 + \alpha_6 \sin(\alpha_7 \theta_s)$ was tried. The residuals of this model showed a weak wavelength dependence. After considerable experimentation the model chosen was

$$\hat{f}_L = \alpha_5 + \alpha_6 \left(\frac{\lambda}{550}\right) \sin(\alpha_7 \theta_s). \tag{26}$$

The best fit values of the coefficients are $\alpha_5 = 1.0247$, $\alpha_6 = 0.4584$ (for λ in nanometers), and $\alpha_7 = 0.1221$ (for θ_s measured in radians). Figure 4 shows the scatterplot for this model. Here 93.0% of the model predictions are within 2% of correct (points lying between the dashed lines); the correlation coefficient is $r = 0.829$. Although it is possible to obtain slightly better fits by including IOPs in an ad hoc fashion, the model of equation (26) was selected because of its simplicity and because of the lack of physical guidance for the IOP dependence.

[29] Although one is unable to model the remaining variability of f_L in terms of the IOPs or other parameters, this may be of little importance in predicting f_L itself because f_L is always near 1. Perhaps more important is the fact that the variability in f_L determines the variability in the fractional forward scattering coefficient $B_f = b_f (1 - f_L)$. Small fractional errors in f_L can cause large fractional errors in B_f. Figure 5 shows the resulting scatterplot for B_f, computed using the exact values of b_f as found in the database. Although 93.0% of the f_L values are within 2% of their correct value, only 5.4% of the B_f values are within 2% of the correct value; 58.1% of the B_f are within 20% of the correct value. However, a percentage error criterion may be misleading for B_f because of the cluster of points near zero, where small absolute errors can be large fractional errors. The dotted lines in Figure 5 thus show absolute errors of ± 0.02 m^{-1}; 94.5% of the B_f have errors smaller than this. The model-actual correlation coefficient is $r = 0.966$.

4.5. Model for *k*

[30] The SSA again suggests a functional form for the $k(\theta, \phi, z = 0)$ model. Differentiating the SSA upwelling radiance of equation (25) gives

$$k(\theta, \phi, 0) = \left[-\frac{1}{L_u(z)} \frac{dL_u(z)}{dz}\right]_{z=0} \approx \frac{c}{\cos(\theta_s)}.$$

Although k is strongly correlated with a ($r = 0.99$), it is not strongly correlated with c ($r = 0.56$). At the level of the quasi-single-scattering approximation (QSSA), which often works well for upwelling radiances, $c \approx a + b_b$, in which case, $k \approx (a + b_b)/\cos(\theta_s)$. This suggested a model k with the functional form

$$\hat{k} = \frac{\alpha_8 a + \alpha_9 b_b}{\cos(\theta_s)}. \tag{27}$$

When equation (27) was used to fit the points in the remote sensing data set, the points separated into distinct groups for $\theta_s \geq 60°$ and for $\theta_s < 60°$. Plots of k and the residual error in k as functions of θ_s suggested that an additive $\sin(\theta_s)$ term would represent the θ_s dependence better than the $1/\cos(\theta_s)$ factor in equation (27). This then gave the final k model:

$$\hat{k} = \alpha_8 a + \alpha_9 b_b + \alpha_{10} \sin(\theta_s). \tag{28}$$

The best fit parameters are $\alpha_8 = 1.0896$, $\alpha_9 = -0.5931$, and $\alpha_{10} = 0.0492$ (for a, b_b, and k in inverse meters). (Note that

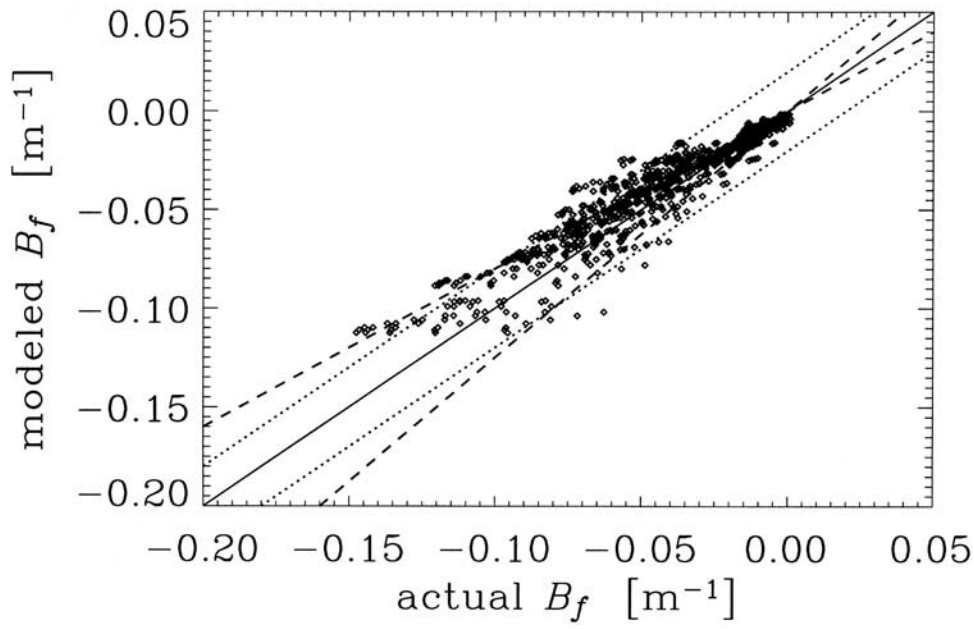

Figure 5. Comparison of modeled and actual B_f values, computed using the f_L model of equation (26). The dashed lines are 20% error bounds; the dotted lines are ±0.02 m^{-1} error bounds.

although θ_s in equation (28) refers to the polar angle of the solar beam in water, the in-air solar zenith angle for θ_s, can be used because the index-of-refraction factor that converts $\sin(\theta_s$ in air) to $\sin(\theta_s$ in water) is incorporated into α_{10}.) The points still separate somewhat by $\theta_s \geq 60°$ and for $\theta_s < 60°$ but not as much as for equation (27). Although equation (28) has lost some of its intuitive, first-order physics, namely the $1/\cos(\theta_s)$ factor in equation (27), the final model does a better job of predicting k, which, of course, is influenced by multiple scattering and other effects not included in the SSA. Figure 6 shows the scatterplot for the k model. Because of small differences near $k = 0$, only 76.8% of the points are within 20% of the correct value. However, 93.6% of the points lie within an absolute error of ±0.05 m^{-1}. The model-actual correlation coefficient is $r = 0.993$.

4.6. Model for $\boldsymbol{R}_\mu$

[31] A model for $\boldsymbol{R}_\mu = \bar{\mu}_d$(in air)/$\bar{\mu}_d$(in water at z = 0) can be constructed simply by using Snell's law to refract the direct solar beam through a level water surface. The result is

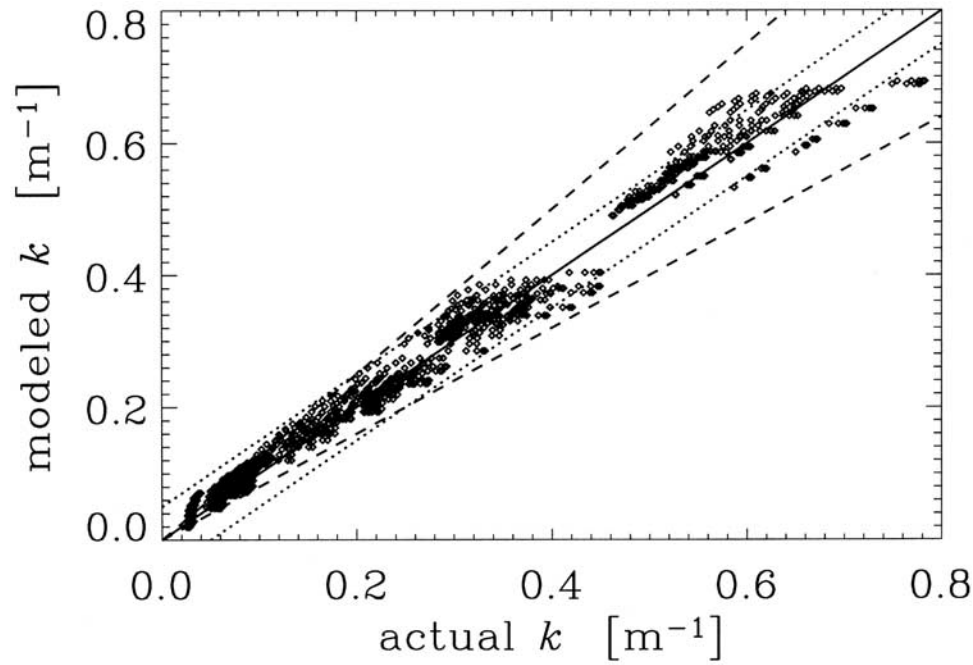

Figure 6. The k model of equation (28). The dashed lines are the 20% error bounds, and the dotted lines are ±0.05 m^{-1} error bounds.

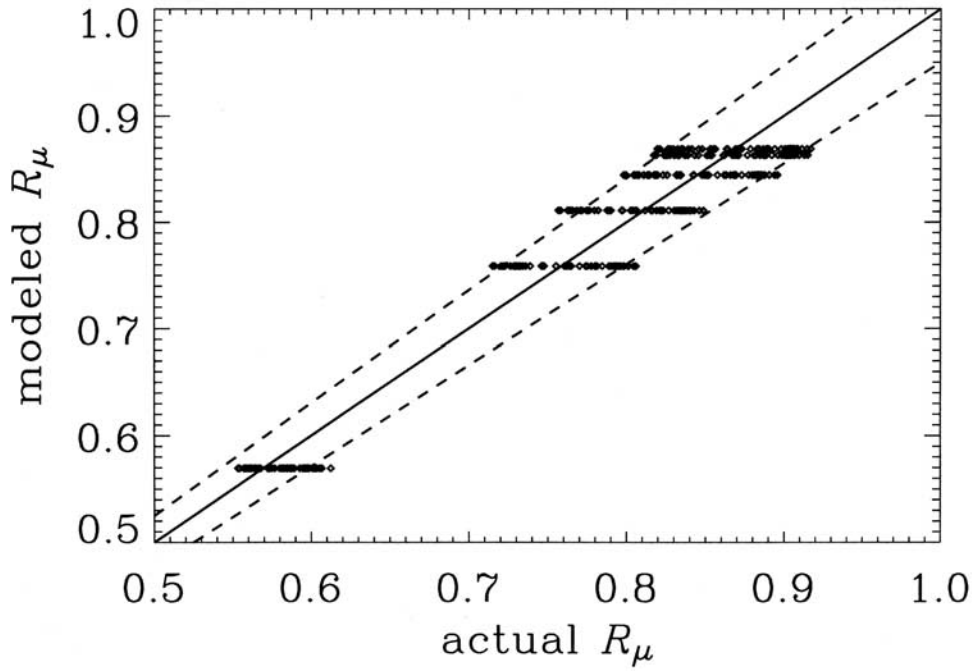

Figure 7. The model of equation (29) applied to the RS data set. The dashed lines are 5% error bounds.

$$\hat{R}_\mu = \alpha_{11} \frac{\cos\theta_s}{\cos\left[\sin^{-1}\left(\frac{\sin\theta_s}{n}\right)\right]} = \alpha_{11}\Theta(\theta_s), \tag{29}$$

where $n = 1.34$ is the index of refraction of water. The ratio R_μ is independent of the viewing direction because the mean cosines are computed from integrals over the direction of the radiance distribution; there are consequently, many fewer distinct points in the data set. When equation (29) is applied to the RS data set, the best fit value is $\alpha_{11} = 0.869$. Figure 7 shows the results of this model applied to all points in the RS data set. The six groups of points correspond to the six solar angles in the data set: $\theta_s = 0$, 10, 20, 30, 40, and 60 degrees. Here 85.7% of the points lie within 5% of the correct value, as shown by the dashed lines. The correlation coefficient is $r = 0.964$.

5. Remotely Sensed Reflectance RSR_a Estimation

[32] Models that estimate the shape factors and related quantities with varying degrees of certainty are now complete. The question next arises as to how well one can predict the remotely sensed reflectance RSR_a using these models within equation (9). Figure 8 gives the answer: 68.1% of the RSR_a predictions fall within 10% of the correct values, and 95.7% fall within 20% of correct (shown by the dashed lines in Figure 8); 85.6% of the predictions are within ± 0.0005 sr^{-1} of the correct value. The model-actual correlation coefficient is $r = 0.983$.

6. Discussion

[33] To facilitate a brief comparison of the shape factor models, propagation of errors into the retrieved IOPs, and discussion of future inversion research, all the models are reassembled below.

$$\hat{f}_b = \alpha_1 + \alpha_4 \frac{b}{b_b}\left[1 + \frac{\alpha_2}{\alpha_4}\cos(\alpha_3\,\xi)\right]. \tag{30}$$

$$\hat{B}_f = b_f\left(1 - \hat{f}_L\right) \quad \textit{where} \quad \hat{f}_L = \alpha_5 + \alpha_6\left(\frac{\lambda}{550}\right)\sin(\alpha_7\theta_s). \tag{31}$$

$$\hat{k} = \alpha_8\, a + \alpha_9\, b_b + \alpha_{10}\sin(\theta_s). \tag{32}$$

$$\hat{R}_\mu = \alpha_{11} \frac{\cos\theta_s}{\cos\left[\sin^{-1}\left(\frac{\sin\theta_s}{n}\right)\right]} = \alpha_{11}\Theta(\theta_s). \tag{33}$$

Although they were derived from a physical basis, it was seen that the models could take various forms. At this early stage of development the above models probably represent the starting point of their eventual evolution.

[34] The highly important $\hat{f}_b$ model contains (1) two IOPs: b_b and b_f (but in a ratio combination $b/b_b = [(b_b + b_f)/b_b] = [1 + b_f/b_b]$), (2) the most model coefficients (four), and (3) the Sun sensor included angle ξ (but not the solar zenith angle θ_s as do all the other models). In contrast, the B_f model contains (1) the solar zenith angle and one IOP (b_f) and (2) the sole wavelength dependence found within the models. The $\hat{k}$ model contains only one IOP, b_b, and the solar zenith angle, θ_s. The $\hat{R}_\mu$ model contains no IOPs; only the solar zenith angle θ_s. (Inversion of the shape factor RTE also requires models for those IOPs that are to be retrieved. For example, the phytoplankton absorption coefficient a_{ph}, the CDOM/detritus absorption coefficient a_d and total constituent backscattering b_{bt} as given in equation (17).

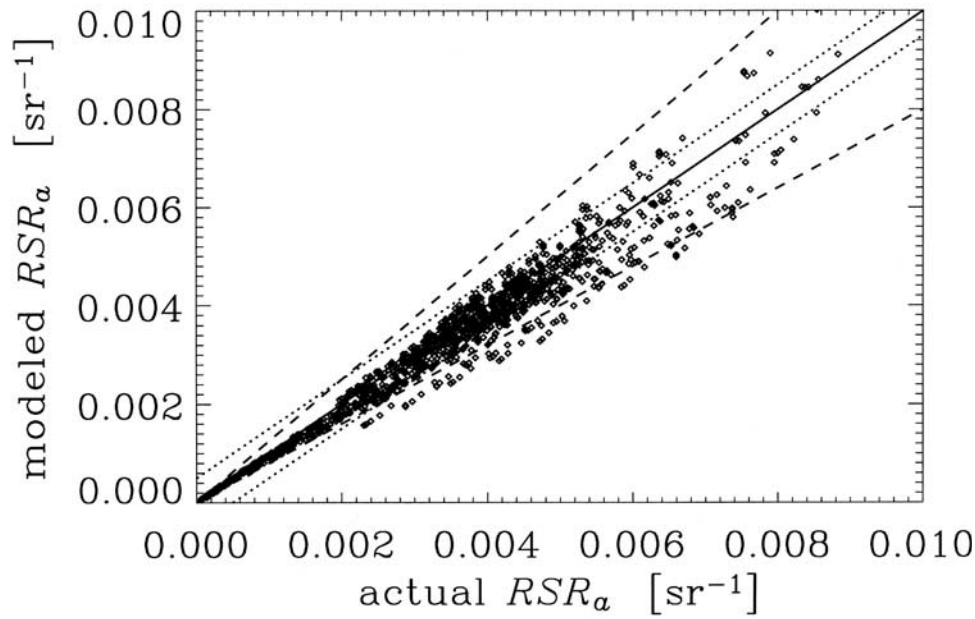

Figure 8. RSR_a as modeled by equation (9) using the four shape factor models. The dashed lines are 20% error bounds; the dotted lines are ±0.0005 sr^{-1}.

These IOP models [*Hoge and Lyon*, 1996] are considered more mature than the shape factor models. Uncertainty propagated into retrieved IOPs by the IOP models used within a semianalytic radiance model inversion has been studied [*Hoge and Lyon*, 1996].)

[35] Thus, to initiate an iterative inversion, starting values are required for both b_b and b_f. Physics demands that $b_b \geq b_{bw}$, where b_{bw} is the backscattering coefficient for water. One possible method for selecting the starting value for b_b is to retrieve it by first executing a semianalytic model inversion [*Hoge and Lyon*, 1996; *Hoge et al.*, 1999a, 1999b, 2001]. Then it can continually be updated after each shape factor RTE inversion in equation (17) since $b_b = b_{bw} + b_{bt}$. Similarly, physics dictates and limits the range of b_f for the first iteration of the shape factor RTE inversion: $b_f \geq b_{fw}$ where b_{fw} is the forward scattering coefficient for water. Although $b_f = b_{fw}$ can perhaps be used as the starting value for the first iteration, future research efforts must develop methods for better (1) selection of starting values and (2) updating of the value during subsequent iterations. Like b_b, the b_f can, in principle, be retrieved using equation (17). This too, however, presents some concerns: (1) few if any models exist for b_f to allow its retrieval by equations (17) and (2) a concurrent retrieval of b_f potentially weakens the retrieval of the desired a_{ph}, a_d, and b_{bt}. Detailed error propagation analyses of the shape factor RTE inversion are outside the scope of this present paper, but a brief discussion of the relative influence of the shape factor models on the desired IOP state vector, $\boldsymbol{p} = [a_{ph}(\lambda_g), a_d(\lambda_d) b_{bt}(\lambda_b)]^T$, is provided in the following section.

6.1. Uncertainties in the IOP State Vector *p*

6.1.1. Sensitivity of *p* to Perturbations in the Data-Model Matrix *D*

[36] As already noted, the inversion of the shape factor form of the RTE is exact from the standpoint of radiative transfer theory, and uncertainties in the retrieved IOPs within the IOP state vector $\boldsymbol{p}$ are due only to the accuracy of the (1) shape factor models and their related quantities and (2) IOP models. Perturbations within $\boldsymbol{D}$ arise, for example, from the water-leaving radiances, scalar irradiances, IOP models, and backscattering shape factor contained within it. Similarly, uncertainties in $\mathbf{h}$ arise from the radiances, irradiances, hydrospheric constants (or IOP constants a_w and b_{bw}) for sea water, as well as f_b, $dL_u(\lambda_i)/dz$, $b_f(\lambda_i)$, $f_L(\lambda_i)$, and cos θ. Relative to $\boldsymbol{h}$, the data-model matrix, $\boldsymbol{D}$, plays the major role in the propagation of errors into $\boldsymbol{p}$ since $\|\boldsymbol{p} - \boldsymbol{p}'\|/\|\boldsymbol{p}\| \leq \kappa(\boldsymbol{D})\,(\|\Delta_{\boldsymbol{D}}\|/\|\boldsymbol{D}\| + \|\delta_{\boldsymbol{h}}\|/\|\boldsymbol{h}\|)$, where $\|\boldsymbol{D}\|$ is the determinate of $\boldsymbol{D}$ and $\kappa(\boldsymbol{D}) = \|\boldsymbol{D}\|\,\|\boldsymbol{D}^{-1}\|$ [*Ortega*, 1990; *Hoge and Lyon*, 1996]. The latter expression is the condition number of $\boldsymbol{D}$, and $\Delta_{\boldsymbol{D}}$ and $\delta_{\boldsymbol{h}}$ represent uncertainty or perturbation of $\boldsymbol{D}$ and $\boldsymbol{h}$, respectively. Here $\boldsymbol{p}'$ is the perturbed solution of $\boldsymbol{p}$. The first expression simply states that to first order the relative error in $\boldsymbol{p}$ can be $\kappa(\boldsymbol{D})$ times the relative error in $\boldsymbol{D}$ and $\boldsymbol{h}$. Thus the propagation into $\boldsymbol{p}$ of the relative errors of both $\boldsymbol{D}$ and $\boldsymbol{h}$ is governed by the condition number of $\boldsymbol{D}$. For any norm, $1 \leq \kappa(\boldsymbol{D}) \leq \infty$. For the limiting cases: $\kappa(\boldsymbol{D}) = 1$, $\boldsymbol{D}$ is said to be perfectly conditioned, while for $\kappa(\boldsymbol{D}) = \infty$, $\boldsymbol{D}$ is singular. For intermediate values of $\kappa(\boldsymbol{D})$ the interpretation of the condition number is very subjective and must be evaluated separately. For large $\kappa(\boldsymbol{D})$ the $\boldsymbol{D}$ matrix is said to be ill conditioned and large errors may be found in $\boldsymbol{p}$. For small $\kappa(\boldsymbol{D})$ the $\boldsymbol{D}$ matrix is said to be well-conditioned and smaller errors may be found in $\boldsymbol{p}$. Of the shape factor components only f_b occurs in $\boldsymbol{D}$ (via V) and therefore provides the strongest influence on the IOP retrieval errors. This is in agreement with *Zaneveld* [1995], who concluded that f_b is most critical since the in-water remotely sensed reflectance (see equation (2)) is directly proportional to it. It is for this reason that shape factor RTE component model developments should probably focus on f_b.

[37] However, if other RTE components such as D_L (or dL_u/dz) and/or B_f are solved for, then they too will appear in the $\boldsymbol{D}$ matrix and thereby further increase the errors in $\boldsymbol{p}$. Also, in general, the condition number increases as the number of unknowns increases [*McCormick*, 1992], contributing still more uncertainty in $\boldsymbol{p}$. In part, the additional uncertainty in $\boldsymbol{p}$ will then be due to D_L and/or B_f model errors. If D_L and B_f are both zero, then equation (13) shows that both R_{rs} and RSR_a are linearly proportional to $b_b/(a + b_b)$, which is a well known *approximate* functional form for the dependence of water-leaving reflectances on the absorption and backscattering coefficients. However, other work [*Gordon et al.*, 1988] suggests, but does not prove, that since the shape factor RTE is exact, both D_L and B_f cannot concurrently be zero. For example, the semianalytic model contains a quadratic term $[b_b/(a + b_b)]^2$, and this suggests that the multiplier $M\frac{f_b(\theta,\phi,0)}{2\pi}R_\mu$ in the numerator of equation (13) above must jointly account for both linear and quadratic variability in $b_b/(a + b_b)$ if both D_L and B_f are null. This comparison to the semianalytic model [*Gordon et al.*, 1988] also suggests, but does not prove, that (1) D_L and B_f (when not being solved for) jointly contribute only a small amount to the reflectances and thus to the IOP retrievals and, (2) accordingly, their contribution to retrieved IOP uncertainty may not be strong.

6.1.2. Sensitivity of *p* to Perturbations in *h*

[38] While the condition of $\boldsymbol{D}$ is most important in determining the errors in the IOP state vector $\boldsymbol{p}$, the error propagation equation, $\|\boldsymbol{p} - \boldsymbol{p}'\|/\|\boldsymbol{p}\| \leq \kappa(\boldsymbol{D})\,(\|\Delta_{\boldsymbol{D}}\|/\|\boldsymbol{D}\| + \|\delta_{\boldsymbol{h}}\|/\|\boldsymbol{h}\|)$, shows that uncertainties in $\boldsymbol{h}$ also propagate into $\boldsymbol{p}$.

6.2. Future Studies

[39] To fully understand how shape factor model errors affect the accuracy of retrieved IOPs, it is necessary to perform in-depth studies of the iterative shape factor inversion algorithm outlined above by (1) its application to synthetic and (2) actual data sets. Thus future research in our laboratories will study the details of the shape factor inversion in a controlled environment such as Hydrolight-generated synthetic RSR_a data, for which the correct IOP values are known from the input to the Hydrolight computer program. The inversion will then be applied to actual RSR_a or R_{rs} field data that further contain experimental errors. Too, the convergence and condition (i.e., well conditioned or ill conditioned) of successive iterations using the retrieved/updated b_f and b_b must also be assessed. Results of these anticipated studies of the inversion of the shape factor RTE are the subject of future publications.

Notation

a total absorption coefficient, $a_t + a_w$, m^{-1}; denotes "in air" when used as a subscript.
a_d absorption coefficient of CDOM and detritus, m^{-1}.
a_{ph} absorption coefficient of phytoplankton, m^{-1}.
a_t total constituent absorption coefficient, $a_t = a_{ph} + a_d$, m^{-1}.
a_w absorption coefficient of water, m^{-1}.
b total scattering coefficient, m^{-1}.
b_b total backscattering coefficient, $b_b = b_{bw} + b_{bt}$, m^{-1}.
b_f total forward scattering coefficient, m^{-1}.
b_{ft} total constituent forward scattering coefficient, m^{-1}.
b_{bt} total constituent backscattering (TCB) coefficient, m^{-1}.
b_{bw} backscattering coefficient of seawater, m^{-1}.
B_f fractional forward scattering coefficient, defined by equation (11), m^{-1}.
B_t b_{bt}/b_t, the total constituent (particle) backscattering fraction.
c beam attenuation coefficient, $c = a + b$, m^{-1}.
CDOM chromophoric dissolved organic matter.
$\boldsymbol{D}$ data and model matrix.
$\|\boldsymbol{D}\|$ determinate of $\boldsymbol{D}$.
D_L radiance derivative term, defined by equation (10), m^{-1}.
$E_{od}(z)$ downwelling scalar irradiance, in water, W m^{-2} nm^{-1}.
E_{oda} downwelling scalar irradiance, in air, just above sea surface, W m^{-2} nm^{-1}.
$E_d(z)$ downwelling plane irradiance, in water, W m^{-2} nm^{-1}.
E_{da} downwelling plane irradiance, in air, W m^{-2} nm^{-1}.
$E_u(z)$ upwelling plane irradiance, in water, W m^{-2} nm^{-1}.
E_{ua} upwelling plane irradiance, in air, W m^{-2} nm^{-1}.
F_{ik} modeling function; contains some subset of the parameters P_k.
f_b backscattering shape factor, dimensionless.
$\hat{f}_b$ estimated backscattering shape factor, dimensionless.
f_L radiance shape factor, dimensionless.
$\hat{f}_L$ estimated radiance shape factor, dimensionless.
$\overline{f_L}$ average of f_L values having θ_s in remote sensing data set.
g phytoplankton Gaussian model spectral width parameter, nm.
$\boldsymbol{h}$ vector of hydrospheric constants, shape factors, radiance attenuation coefficient, m^{-1}.
IOP inherent optical property.
K_{Lu} diffuse attenuation coefficient for upwelling radiance, $K_{Lu} = -\mathrm{d}[\log L_u(z, \theta, \phi)]/\mathrm{d}z$.
L_u upwelling radiance, below sea surface, W m^{-2} sr^{-1} nm^{-1}.
L_{ua} upwelling radiance, in air, just above sea surface, W m^{-2} sr^{-1} nm^{-1}.
M $[(\bar{t}\bar{t})/[(1 - rR)n_w^2] \approx 0.54$ for nominal sea conditions, dimensionless.
n total constituent backscattering coefficient spectral model exponent, as used in equation (17), dimensionless.
n_w index of refraction of sea water, dimensionless.
P_k modeling parameter; $k = 1,\ldots, N_k$, denote the parameters (wavelength, viewing direction, IOPs, etc) to be used in modeling the X_i.
$\boldsymbol{p}$ oceanic state vector of retrieved IOPs, $^{-1}$.
$\boldsymbol{p}'$ perturbed oceanic state vector of retrieved IOPs, $^{-1}$.
$\|\boldsymbol{p}\|$ determinate of $\boldsymbol{p}$.
r water-to-air surface reflectance for plane irradiance, dimensionless; correlation coefficient when specifically identified.
R plane irradiance reflectance, in water, $E_u(z)/E_d(z)$, dimensionless.
R_μ ratio of air-to-water mean cosines for downwelling irradiance.

$\hat{R}_\mu$ estimate of ratio of air-to-water mean cosines for downwelling irradiance.
RSR remotely sensed reflectance, in-water, $L_u(\theta, \phi, z)/E_{od}(z)$, sr^{-1}.
RSR_a remotely sensed reflectance, in air, $L_{ua}(\theta, \phi)/E_{oda} = \bar{\mu}_{da}R_{rs}$, sr^{-1}.
R_{rs} remote sensing reflectance, in air, $L_{ua}(\theta, \phi)/E_{da}$, sr^{-1}.
RTE radiative transfer equation.
s subscript denoting solar; used in subscript *rs* denotes remote sensing.
S spectral slope within the a_d model for CDOM+detritus, nm^{-1}.
t water-to-air radiance transmittance, dimensionless.
$\bar{t}$ water-to-air plane irradiance transmittance, dimensionless.
TCA total constituent absorption, a_t, m^{-1}.
TCB total constituent backscattering, b_{bt}, $^{-1}$.
v subscript; italicized letter "v" denoting viewing.
V backscattering enhancement factor, defined by equation (12), dimensionless.
X_i shape factors and related quantities; i = 1, 2, 3, and 4, denote f_b, f_L, k, and R_μ respectively.
z depth, m.
α_i model fitting parameters, see text and tables for numerical values.
α_{ik} model fitting coefficients; a different set of coefficients is needed for each factor X_i.
β volume scattering function.
δ Dirac delta function.
$\Delta_{\boldsymbol{D}}$ uncertainty or perturbation of $\boldsymbol{D}$.
$\|\Delta_{\boldsymbol{D}}\|$ determinate of $\Delta_{\boldsymbol{D}}$.
$\delta_{\boldsymbol{h}}$ uncertainty or perturbation of $\boldsymbol{h}$.
$\|\delta_{\boldsymbol{h}}\|$ determinate of $\delta_{\boldsymbol{h}}$.
$\kappa(\boldsymbol{D})$ $\|\boldsymbol{D}\|\ \|\boldsymbol{D}^{-1}\|$, the condition number of $\boldsymbol{D}$.
λ wavelength, nm.
λ_b reference λ for total constituent backscattering (TCB) coefficient model, nm.
λ_d reference wavelength for CDOM+detritus absorption coefficient model, nm.
λ_g peak wavelength for Gaussian phytoplankton absorption coefficient model, nm.
λ_i wavelength of observational bands, i = 1, 2, 3, . . ., nm.
ν italicized Greek letter nu is not used in this paper: see italicized letter "v" above.
$\bar{\mu}_d$ average cosine for downwelling irradiance, in water, dimensionless.
$\bar{\mu}_{da}$ average cosine for downwelling irradiance, in air, dimensionless.
ϕ azimuth angle, radians; subscripts *v*, *s* denote viewing, solar.
θ polar zenith angle in-water with respect to +*z* axis, radians; subscripts *v*, *s*, and *a* denote viewing, solar, and in-air, respectively.
ξ included angle, solar-to-viewing direction.
ω_o single-scattering albedo *b*/*c*.

[40] **Acknowledgments.** The continued support and encouragement of NASA Headquarters Ocean Biology Program as well as the EOS Project Office is gratefully acknowledged. Authors C. D. M. and L. K. S. were also supported by the Environmental Optics Program of the Office of Naval Research under contract N-00014-01-M-0268. Two reviews by J. Ronald V. Zaneveld greatly improved the manuscript.

References

Davis, C. O., et al., Ocean PHILLS hyperspectral imager: Design, characterization, and calibration, *Opt. Express*, *10*, 210–221, 2002.
Gordon, H. R., Modeling and simulating radiative transfer in the ocean, in *Ocean Optics*, edited by R. W. Spinrad, K. L. Carder, and M. J. Perry, chap. 1, pp. 3–39, Oxford Univ. Press, New York, 1994.
Gordon, H. R., O. B. Brown, R. H. Evans, J. W. Brown, R. C. Smith, K. S. Baker, and D. K. Clark, A semianalytic radiance model of ocean color, *J. Geophys. Res.*, *93*, 10,909–10,924, 1988.
Hoge, F. E., and P. E. Lyon, Satellite retrieval of inherent optical properties by linear matrix inversion of oceanic radiance models: An analysis of model and radiance measurement errors, *J. Geophys. Res.*, *101*, 16,631–16,648, 1996.
Hoge, F. E., and P. E. Lyon, Satellite observation of chromophoric dissolved organic matter (CDOM) variability in the wake of hurricanes and typhoons, *Geophys. Res. Lett.*, *29*(19), 1908, doi:10.1029/2002GL015114, 2002.
Hoge, F. E., C. W. Wright, P. E. Lyon, R. N. Swift, and J. K. Yungel, Satellite retrieval of inherent optical properties by inversion of an oceanic radiance model: A preliminary algorithm, *Appl. Opt.*, *38*, 495–504, 1999a.
Hoge, F. E., C. W. Wright, P. E. Lyon, R. N. Swift, and J. K. Yungel, Satellite retrieval of the absorption coefficient of phytoplankton phycoerythrin pigment: Theory and feasibility status, *Appl. Opt.*, *38*, 7431–7441, 1999b.
Hoge, F. E., C. W. Wright, P. E. Lyon, R. N. Swift, and J. K. Yungel, Inherent optical properties imagery of the western North Atlantic Ocean: Horizontal spatial variability of the upper mixed layer, *J. Geophys. Res.*, *106*, 31,129–31,140, 2001.
McCormick, N. J., Inverse radiative transfer problems: A review, *Nucl. Sci. Eng.*, *112*, 185–198, 1992.
Mobley, C. D., *Light and Water, Radiative Transfer in Natural Waters*, Academic, San Diego, Calif., 1994.
Mobley, C. D., *Hydrolight 4. 2 Users' Guide*, 88 pp., Sequoia Sci., Redmond, Wash., 2001a. (Available at www.sequoiasci.com.)
Mobley, C. D., *Hydrolight 4. 2 Technical Documentation*, 79 pp., Sequoia Sci., Redmond, Wash., 2001b.
Mobley, C. D., B. Gentili, H. R. Gordon, Z. Jin, G. W. Kattawar, A. Morel, P. Reinersman, K. Stamnes, and R. H. Stavn, Comparison of numerical models for computing underwater light fields, *Appl. Opt.*, *32*, 7484–7504, 1993.
Morel, A., and B. Gentili, Diffuse reflectance of oceanic waters. III. Implication of bidirectionality for the remote sensing problem, *Appl. Opt.*, *35*, 4850–4862, 1996.
O'Reilly, J., S. Maritorena, B. G. Mitchell, D. A. Siegel, K. L. Carder, S. A. Garver, M. Kahru, and C. McClain, Ocean color chlorophyll algorithms for SeaWiFS, *J. Geophys. Res.*, *103*, 24,937–24,953, 1998.
Ortega, J. M., Numerical analysis, in *A Second Course*, Soc. for Ind. and Appl. Math., Philadelphia, Pa., 1990.
Pope, R. M., and E. S. Fry, Absorption spectrum (380–700 nm) of pure water: II. Integrating cavity measurements, *Appl. Opt.*, *36*, 8710–8723, 1997.
Smith, R. C., and K. S. Baker, Optical properties of the clearest natural waters (200–800 nm), *Appl. Opt.*, *20*, 177–183, 1981.
Weidemann, A. D., R. H. Stavn, J. R. V. Zaneveld, and M. R. Wilcox, Error in predicting hydrosol backscattering from remotely sensed reflectance, *J. Geophys. Res.*, *100*, 13,163–13,177, 1995.
Zaneveld, J. R. V., Remotely sensed reflectance and its dependance on vertical structure: A theoretical derivation, *Appl. Opt.*, *21*, 4146–4150, 1982.
Zaneveld, J. R. V., A theoretical derivation of the dependance of the remotely sensed reflectance of the ocean on the inherent optical properties, *J. Geophys. Res.*, *100*, 13,135–13,142, 1995.

F. E. Hoge, National Aeronautics and Space Administration, Goddard Space Flight Center, Wallops Flight Facility, Wallops Island, VA 23337, USA. (frank.hoge@nasa.gov)
P. E. Lyon, E. G. & G. Inc., Wallops Flight Facility, Wallops Island, VA 23337, USA.
C. D. Mobley and L. K. Sundman, Sequoia Scientific, Inc., Westpark Technical Center, 15317 NE 90th Street, Redmond, WA 98052, USA.